



EXPERIMENTAL AND NUMERICAL STUDY OF THE PRESSURE OF THE WATER FLOW IN A VENTURI TUBE

ESTUDIO EXPERIMENTAL Y NUMÉRICO DE LA PRESIÓN DEL FLUJO DE AGUA EN UN TUBO VENTURI

San Luis B. Tolentino Masgo^{1,2}

Abstract

The Venturi tube is a device used to measure the flow rate in different industrial processes. In the present work, a study is carried out for two cases, one experimental and another numerical of the pressure exerted by the flow of water on the walls of a Venturi tube. In the first case, five experiments with different flow rates are carried out. In the second, the flow is simulated for two types of meshes and two turbulence models, using the code COMSOL Multphysics 4.3. The experimental and numerical results showed that the pressures of the flow on the walls in two references identified as C and G keep their magnitude constant; in addition, the numerical profiles showed that the lowest pressure drop occurs in the wall at the inlet and outlet of the throat section. It is concluded that, the distribution of the flow pressure in the wall of the throat section has a convex profile, and the results of pressures obtained for the standard $k - e$ turbulence model are more adjusted to the experimental data.

Keywords: Water flow, Turbulence model, Pressure, Simulation, Venturi tube.

Resumen

El tubo Venturi es un dispositivo utilizado para medir el caudal en diferentes procesos de la industria. En el presente trabajo, se realiza un estudio para dos casos, uno experimental y otro numérico de la presión ejercida por el flujo de agua en las paredes de un tubo Venturi. En el primer caso, se realizan cinco experimentos con diferentes caudales. En el segundo, el flujo se simula para dos tipos de mallas y dos modelos de turbulencia, utilizando el código COMSOL Multphysics 4.3. Los resultados experimentales y numéricos mostraron que las presiones del flujo sobre las paredes en dos referencias identificadas C y G mantienen constante su magnitud; además, los perfiles numéricos mostraron que la menor caída de presión se presenta en la pared a la entrada y salida de la sección de la garganta. Se concluye que, la distribución de la presión del flujo en la pared de la sección de la garganta tiene un perfil convexo, y los resultados de presiones obtenidos para el modelo de turbulencia $k-e$ estándar, se ajustan más a los datos experimentales.

Palabras clave: flujo de agua, modelo de turbulencia, presión, simulación, tubo Venturi.

^{1,*}Department of Mechanical Engineering, Universidad Nacional Experimental Politécnica “Antonio José de Sucre” Vice-Rectorado Puerto Ordaz, Bolívar, Venezuela.

²Group of Mathematical Modelling and Numerical Simulation, Universidad Nacional de Ingeniería, Lima, Perú.
Corresponding author ✉: sanluis@gmail.com <http://orcid.org/0000-0001-6320-6864>

Received: 28-06-2019, accepted after review: 29-10-2019

Suggested citation: Tolentino Masgo, San Luis B. (2020). «Experimental and numerical study of the pressure of the water flow in a venturi tube». INGENIUS. N.º 23, (january-june). pp. 9-. DOI: <https://doi.org/10.17163/ings.n23.2020.01>.

1. Introduction

In the field of engineering, the instruments used to measure the flow rate of a fluid are classified in two types, mechanical instruments and pressure loss instruments [1, 2], and are described in detail in a book by ASME [3]. The Venturi tube is among the latter as the pressure loss occurs in a constricted section, and was invented by Clemens Herschel (1842-1930) [4], and named after Giovanni Battista Venturi (1746-1822) for his pioneering works about flow in conic sections [2].

The flows in such instruments are, mostly, turbulent, and characterized by having random and rapid fluctuations of eddies, which transport mass, energy and momentum to other regions of the flow, where the fluctuations add movement and energy transfer and, besides, are related to high values of friction coefficients, heat transfer and mass transfer [1, 2].

By means of the dimensionless Reynolds number [5, 6] it is determined if the flow is laminar or turbulent, where the Reynolds number is the parameter that express the relationship between the inertia and viscous forces in a fluid, being the inertia force the product of the average speed and the internal diameter, and of the viscous force the kinematic viscosity. The flow is considered as laminar for a value of the Reynolds number smaller than 2300, as transitional for a value of the Reynolds number in the range 2300-4000, and as turbulent for a value of the Reynolds number greater than 4000, thus resulting in the graphical representation known as Moody diagram [1, 2]. Other studies carried out on conditioned surfaces report that the Reynolds number takes different values for laminar and turbulent flow.

In order to reproduce the behavior of the flow by means of computational fluid dynamics (CFD) [7], experimental data are required for its calibration and validation, such as: pressure, temperature, velocity, which are parameters that can be measured in the laboratory or in open spaces. Besides, the CFD requires utilizing a turbulence model that solves the closure problem in the averaged equations of the Navier-Stokes general equations. Among the diversity of turbulence models for the flow of fluids, the profiles of the numerical solutions that better fit the experimental results should be chosen. Once the turbulence model has been evaluated, it is possible to continue developing the desired computational simulations to determine the behavior of the flow field under certain considerations, whether for internal or external flow. It is worth noting that, in certain critical regions, the numerical results evaluated with different turbulence models [8] are distinct, and in less critical regions the results are similar, due to the boundary layer and the interaction of the flow separation [9, 10].

An experimental research was carried out by Lindley [11] about the transit of flow in a classical Venturi

tube, where at the beginning of the throat section, the water flow experienced pressure drops in a section of the wall. Afterwards, for the same geometry, Sattery and Reader [12] simulated the flow through CFD, where in the throat section the numerical profiles showed pressure drops. A similar result of the pressure drop was also obtained by Tamhakar *et al.* [13], applying CFD, for a Venturi tube of different dimensions. Whereby, this constitutes a motivation for continuing investigating about the pressure of the flow in Venturi meters.

In the present work, an experimental and numerical study is carried out about the pressure exerted by the flow of water on the walls of a Venturi tube. In the experimental case the study was conducted for five experiments with different flow rates, and in the numerical case the study is conducted for two turbulence models: standard $k - \epsilon$ of Launder and Spalding [14] and standard $k - \omega$ of Wilcox [15], and for two domains discretized by the finite elements method (FEM), one with quadrilateral cells and another with triangular cells, in order to determine what regions of the flow experience the minimum pressure drops. Similarly, validate the two turbulence models with the experimental data of pressure. It is worth noting that the experimental values of pressure are measured at specific points that are separated from each other by a defined distance along the wall of the Venturi tube, and does not provide information about pressure in critical sections; while, the numerical profiles are continuous trajectories and provide more information about the pressure along the entire wall.

The mathematical foundation is presented, and the procedures and results of the experiments and of the numerical simulations are exposed. Afterwards, the conclusions of the analysis are presented.

2. Materials and methods

2.1. Experimental facility

The Venturi tube under study in this work is shown in Figure 1. It is a device manufactured by the company TecQuipment, which is utilized in experimental tests to determine the water flow rate by the pressure difference. The experimental equipment is installed in the laboratory of the Section of Thermal Fluids of the Mechanical Engineering Department of the National Experimental Polytechnic University “Antonio José de Sucre”, Puerto Ordaz Vice-Rectorate, Bolívar, Venezuela. The Venturi tube comprises five sections: a straight section, a convergent section, a straight section which is the throat, a divergent section and another straight section. The image shows a total of eleven plastic hoses, called piezometric pipes, which measure the readings of piezometric heights of the water columns, and are connected to the Venturi tube and to the glass

manifold. The control valve is located at the outlet of the Venturi tube, and the purge valve is located at the right end of the collector. The valve for regulating the flow rate is ahead of the Venturi tube and after the pump, which is not shown in the figure.

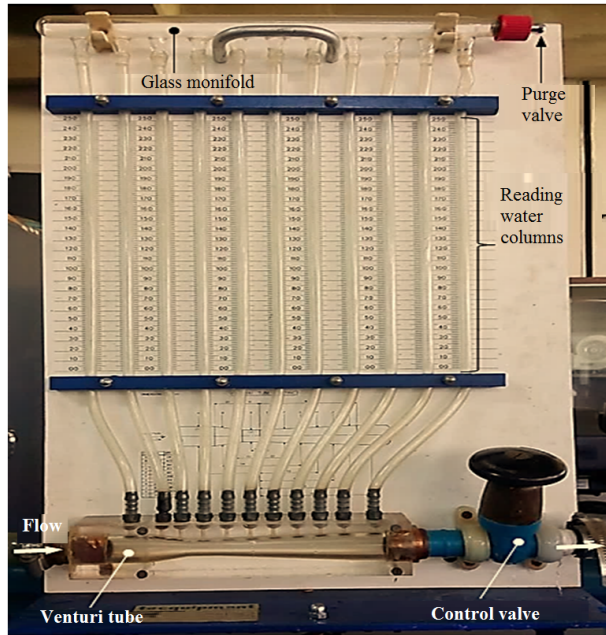


Figure 1. Venturi tube experimental equipment. The readings of the water columns are measured in millimeters.

The 3D geometry and the projection on the plane of the Venturi tube are illustrated in Figure 2, which also shows the location of the references A, B, C, D, E, F, G, H, J, K and L, places to where the eleven plastic hoses are connected. Reference A is located at the beginning of the straight section; B and C are located in the convergent section; D in the middle of the straight section of the throat; E, F, G, H, J and K are located in the divergent section; and L is located at the end of the straight section, at the outlet of the Venturi tube. The greater internal diameter of the two straight sections is 26 mm, the internal diameter of the throat is 16 mm, and the total length of the Venturi tube is 156 mm. The internal diameters of the cross sections and of the locations of the references are shown in Table 1.

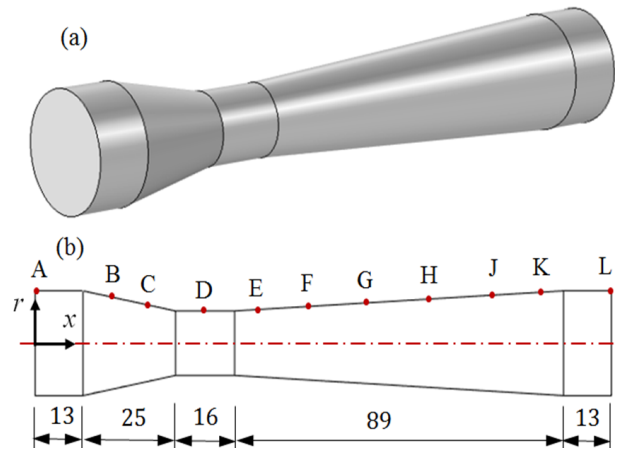


Figure 2. (a) 3D geometry of the Venturi tube. (b) Location of the references and dimensions of the longitudinal sections in millimeters.

Table 1. Internal diameter for each reference, and axial distance where the references are located

Ref.	Internal diameter (mm)	Axial distance, x axis (mm)
A	26	0
B	23,2	20
C	18,4	32
D	16	46
E	16,8	61
F	18,47	76
G	20,16	91
H	21,84	106
J	23,53	121
K	25,24	136
L	26	156

The experimental test was carried out through the following steps: initially, both valves, the valves for flow rate regulation and for flow rate control, were opened at 100 %. Once the pump of the test bench was in operation, the control valve was closed 100 %, the air trapped in the hoses and in the collector was let out through the purge valve leaving it totally full of water; subsequently, the regulation valve was closed 100 %. Then the control valve was opened 100 %, and through the purge valve air from the local atmosphere was let in, thus allowing the formation of water columns at the established height of 140 mm as initial position, all at the same level, for the eleven hoses. The reading of 140 mm remained inside the range of 0.0-200 mm of the panel, as shown in Figure 3. Afterwards, five experimental tests were carried out increasing the opening of the regulation valve, for visually taking the piezometric readings for the range of flow rate $2,244 \times 10^{-4} - 3,7 \times 10^{-4} \text{ (m}^3/\text{s)}$.

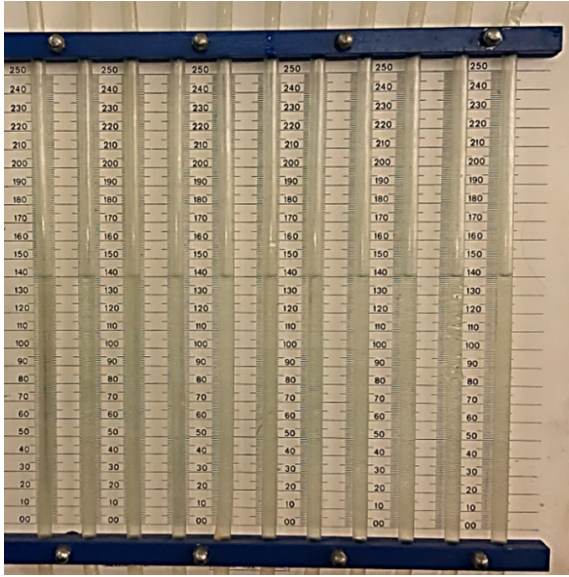


Figure 3. Initial position of the piezometric heights of 140 mm of the levels of the eleven water columns. From left to right, the first piezometric tube is connected in the reference A of the wall of the Venturi tube, the second in the reference B, and similarly, the remaining are located up to the reference L (see Figure 2).

2.2. Numerical simulation

2.2.1. Governing equations

The governing equations applied to the CFD, for an incompressible flow, in stationary conditions, and simulated for a 2D computational domain with axial symmetry, in their differential form are expressed as:

Equation of conservation of mass.

$$\frac{\partial}{\partial x}(\rho v_x) + \frac{\partial}{\partial r}(\rho v_r) + \frac{\rho v_r}{r} = 0 \quad (1)$$

Equation of conservation of linear momentum, in the axial direction.

$$\begin{aligned} \frac{1}{r} \frac{\partial}{\partial x}(r \rho v_x v_x) + \frac{1}{r} \frac{\partial}{\partial r}(r \rho v_r v_x) &= -\frac{\partial P}{\partial x} + \\ \frac{1}{r} \frac{\partial}{\partial x} \left[r \mu \left(2 \frac{\partial v_x}{\partial x} - \frac{2}{3} (\nabla \cdot \vec{v}) \right) \right] + & \\ \frac{1}{r} \frac{\partial}{\partial r} \left[r \mu \left(\frac{\partial v_x}{\partial r} + \frac{\partial v_r}{\partial x} \right) \right] + F_x & \end{aligned} \quad (2)$$

in the radial direction.

$$\begin{aligned} \frac{1}{r} \frac{\partial}{\partial x}(r \rho v_x v_r) + \frac{1}{r} \frac{\partial}{\partial r}(r \rho v_r v_r) &= -\frac{\partial P}{\partial r} + \\ \frac{1}{r} \frac{\partial}{\partial r} \left[r \mu \left(\frac{\partial v_r}{\partial x} - \frac{\partial v_x}{\partial r} \right) \right] - 2 \mu \frac{v_r}{r^2} + \frac{2}{3} \frac{\mu}{r} (\nabla \cdot \vec{v}) + & \\ \frac{1}{r} \frac{\partial}{\partial r} \left[r \mu \left(2 \frac{\partial v_r}{\partial r} - \frac{2}{3} (\nabla \cdot \vec{v}) \right) \right] + F_r & \end{aligned} \quad (3)$$

with $\nabla \cdot \vec{v} = \frac{\partial v_x}{\partial x} + \frac{\partial v_r}{\partial r} + \frac{v_r}{r}$

where the parameters are: the density ρ , the axial velocity v_x and radial velocity v_r , the radius r , the viscosity μ , the pressure gradients $\frac{\partial P}{\partial x}$ and $\frac{\partial P}{\partial r}$, and the forces in the axial direction F_x and in the radial direction F_r .

The turbulence model is coupled to the equation of linear momentum, and are semi-empirical transport equations that model the mixing and diffusion that increase because of the turbulent eddies, and are solved through the Reynolds average number Navier-Stokes equation (RANS) [16]. The initial research studies about turbulence were conducted by Kolmogorov (1941), based on the results obtained by Reynolds (1883). It is worth noting that the turbulence models standard k-e of Launder and Spalding [14] and standard k- ω of Wilcox [15], are employed in the present work for the simulation of the flow.

2.2.2. Computational domain and mesh

The 2D computational domain with axial symmetry shown in Figure 4 is considered, due to the symmetry of the geometry of the Venturi tube. This simplification of the geometry from 3D to 2D contributes to reduce the number of cells in the mesh, the processing time, and the computational cost; the simplifications are very common for solids of revolution and symmetric primitive geometries. Besides, in the same figure of the 2D domain, the places where the boundary conditions are applied have been marked.

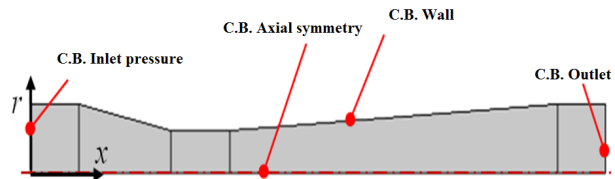


Figure 4. 2D computational domain with axial symmetry in the x axis, of the Venturi tube.

Figure 5 shows the 2D meshed domain, in which two types of cells are used, quadrilateral and triangular. The domain meshed with quadrilateral cells has 19600 elements, and the domain meshed with triangular cells 18047 elements. For both cases, the mesh was refined in the regions adjacent to the walls, due to the presence of shear stresses in those regions of flow. The throat section is also shown in detail in the same figure, where it is observed how the quadrilateral and triangular cells are distributed.

As part of a study of the numerical convergence, before obtaining the final mesh which is shown in Figure 5, the throat section was refined five times until obtaining an optimum mesh density. Such refinement in the throat was because this is a critical section due to pressure drop in the flow. The reference D is located in the middle of the throat length

(see Figure 2), where the final numerical result of the pressure was 44.79 (mmH₂O) for the mesh with quadrilateral cells and 51.38 (mmH₂O) for the mesh with triangular cells, evaluated with the standard $k - e$ turbulence model; and the pressure was 48.53 (mmH₂O) for the mesh with quadrilateral cells and 55.75 (mmH₂O) for the triangular cells, evaluated with the standard $k - \omega$ turbulence model; obtaining for both cases numerical convergence errors smaller than 0.01 %.

The quality of the mesh was evaluated for two-dimensional cells, where for the case of quadrilateral cells it was obtained a maximum element size of 0.0105 mm, a minimum element size of 4.68×10^{-5} mm, a curvature of 0.3, and a rate of increase of 1.3; similarly, for the case of triangular cells it was obtained a maximum element size of 3.64×10^{-4} mm, a minimum element size of 5.2×10^{-5} mm, a curvature of 0.25, and a rate of increase of 1.15. These final results indicate that the two domains meshed with quadrilateral and triangular cells are of good quality.

The computational domains were discretized in the mesh platform of the code COMSOL Multiphysics version 4.3, which applies the finite element method (FEM).

The boundary conditions for the pressures of the water flow applied at the inlet (reference A) and at the outlet (reference L) of the Venturi tube, are shown in Table 2.

The walls of the Venturi tube are considered adiabatic. The velocity of the flow at the walls in the radial and axial direction is zero due to the presence of shear stresses. In the axial symmetry in the x axis, the velocity of the flow in the radial direction is zero.

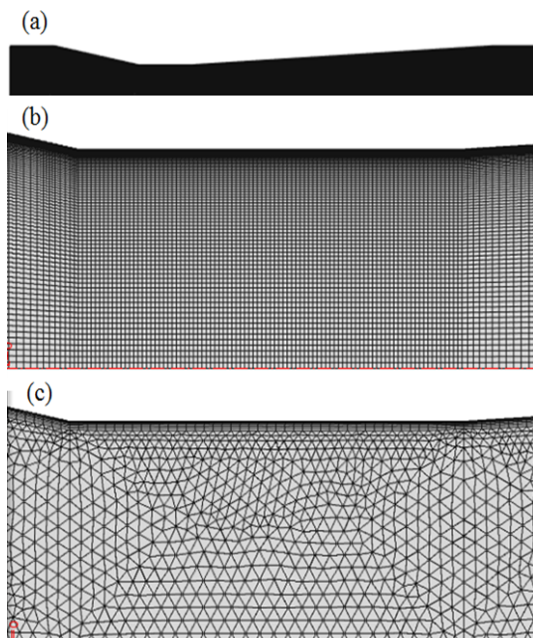


Figure 5. (a) Meshed 2D computational domain. Detail of the throat section, (b) Structured mesh with quadrilateral cells, (c) Mesh with triangular cells.

Isothermal flow is considered along the entire computational domain, and for a water temperature of 24 °C the density was 997.1015 kg/m³ and the dynamic viscosity 0.00091135 Pa.s, where both physical parameters are set as constants for the simulation of the flow.

Table 2. Boundary conditions: inlet pressure (reference A), outlet pressure (reference L)

Exp.	1	2	3	4	5
Water column (mmH₂O)					
Ref. A	160	170	179	190	199,5
Ref. L	150	155,5	161	167	173

2.2.3. Method of computational solution and equipment

A 2D geometry with axial symmetry and stationary flow conditions, was chosen as the option for the simulation of the isothermal flow in the COMSOL Multiphysics code. The turbulence models standard $k - e$ and standard $k - \omega$ were applied for the turbulent flow, for the domains meshed with both quadrilateral and triangular cells. A fixed value of 0.001 was determined for the relative tolerance. For the solution, the maximum number of iterations was established as 100, and the solution method parallel sparse direct solver (PARDISO) was employed.

For data processing, an equipment with the following characteristics was utilized: Siragon Laptop, model M54R, Intel Core 2 Duo, two 1.8 GHz processors, and a RAM memory of 3 GB.

3. Results and discussion

3.1. Experimental results

For each experiment that was carried out, the flow rates of the water were obtained by means of the volumetric method, and the results are shown in Table 3. The Reynolds number was determined with these values of flow rate.

Table 3. Experimental data of flow rates

Exp.	1	2	3	4	5
Caudal $\times 10^4$ (m³/s)					
	2,244	2,583	2,991	3,382	3,704

Table 4 presents the magnitudes of the Reynolds number obtained in the references A, L and D. In reference A the Reynolds number has the same magnitude than in reference L, and this is because the Venturi tube has the same diameter. For the five experiments,

the Reynolds number obtained in the references A and L was in the range $12000 < Re < 20000$, and in the throat section, in the reference D, was in the range $19500 < Re < 32300$. Whereby, it is observed that as the flow rate increases, the magnitude of the Reynolds number also increases, and this is due to the increase in the fluid inertial forces.

Table 4. Experimental data of the Reynolds number

Exp.	1	2	3	4	5
Reynolds number					
Ref. A and L	12021	13839	116028	18118	19844
Ref. D	19534	22489	26045	29442	32246

Table 5 shows the five experimental results of the piezometric heights obtained in the references A, B, C, D, E, F, G, H, J, K and L, Figure 6 shows the graph of the gauge pressure in (mmH₂O), and Figure 7 shows an image of the piezometric heights of the eleven water columns corresponding to experiment 3, and it is observed the concave shape of the menisci due to the effect of the surface tension of the water that is formed in each column.

Taking as reference the initial position of the eleven columns with the water level at the height of 140 mm, it is observed that as the flow rate increases, the level of the water columns in the references A and B increases; in the reference C remains constant; in the references D, E and F decreases; in the reference G it also remains constant; and in the references H, J, K and L increases. Taking into account the differences of the water columns between A and D, the smallest pressure difference occurs for experiment 1, and the largest difference for experiment 5. The losses in the fluid pressure in the reference L with respect to the reference A are also observed in Figure 6. Among all experiments that were carried out, the one with the largest pressure loss is experiment 5.

Table 5. Experimental data of gauge pressure in each reference of the wall of the Venturi tube Temperature of the water: 24 °C

Exp.	1	2	3	4	5
Ref. Water column (mmH ₂ O)					
A	160	170	179	190	199,5
B	156,5	165	172	181	189
C	139,5	139,5	139,5	139,5	139,5
D	106	91	76,5	60,5	45
E	109,5	97	85	72	60
F	125	122	119	115,5	112
G	136	136	136	136	136
H	142	144,5	146,5	150	152
J	145,5	149,5	153	158	162
K	148	153	157,5	163,5	168,5
L	150	155,5	161	167	173

For each experiment, the pressure drop appears in the throat section, as it is shown in the reference D, where the fluid is forced to have a pressure drop, which is known as Venturi effect, and the smallest pressure drop occurs for experiment 5.

Among the results obtained in the references C, where the internal diameter is 18.4 mm, and G where the diameter is 20.16 mm, even though the flow velocity increases in those references due to the increase of the flow rate, the magnitude of the pressures do not vary coming together to a unique place for each reference. This occurs because the control valve remains open at 100 % and the flow is discharged in a reservoir at the local atmospheric pressure, and simultaneously the pressure of the air trapped in the collector, which is smaller than the local atmospheric pressure, holds the formation of the water columns.

It is worth to mention that, if the opening of the regulation valve is kept constant and the control valve is manipulated, there would be no interception in the references C and G, because the level of the water columns would move up or down due to the increase or decrease of the pressure of the flow in all the system of the Venturi tube.

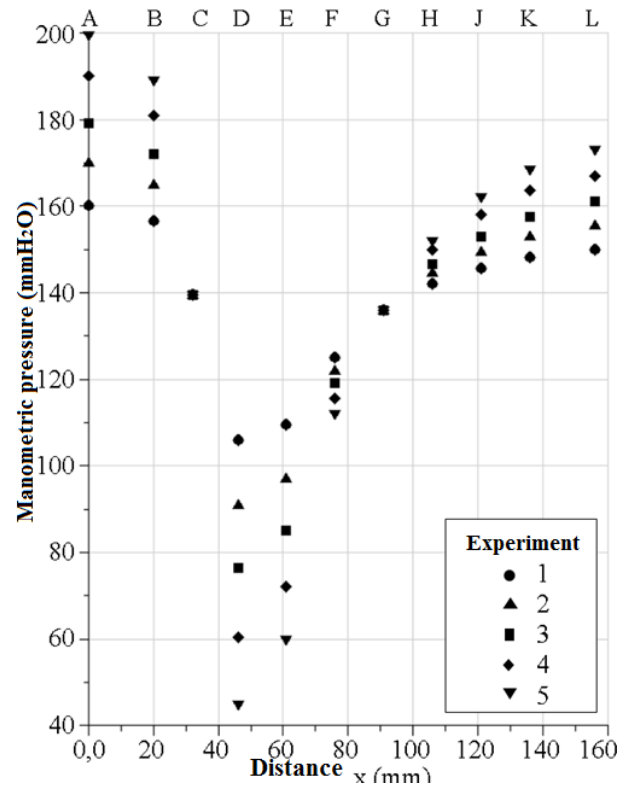


Figure 6. Experimental data of readings of the piezometric heights of the water columns taken at different reference points of the walls of the Venturi tube Temperature of the water 24 °C.

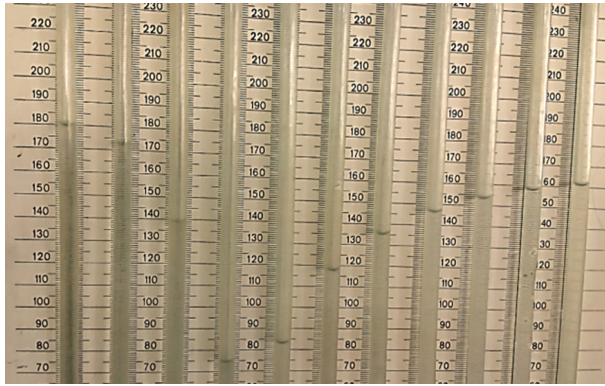


Figure 7. Piezometric heights for different levels of the water columns, corresponding to experiment 3.

On the other hand, if the pressure loss from the reference C to the reference G is analyzed, the pressure drop remains invariant even though the kinetic energy of the fluid is increased in such regions because, as shown in Table 5 and plotted in Figure 6, there is a fixed piezometric height of 139.5 mm in the reference C and of 136.0 mm in the reference G, where the pressure difference is 3.5 (mmH₂O) for the five experiments that were conducted.

The pressure differences between the references A-D and A-L are presented in Table 6, and Figure 8 shows the behavior of both straight lines by means of the linear trend line, which has a determination coefficient $R^2=0.997$ for the A-D pressure difference, and a value $R^2=0.996$ for the A-L pressure difference. Both results show that there is a proportionality of pressure difference with respect to the flow rate.

Table 6. Pressure difference between the references A and D, and the references A and L, for each experiment

Exp.	1	2	3	4	5
ΔP mmH ₂ O					
Ref. A-D	54	79	102,5	129,5	154,5
Ref. A-L	10	14,5	18	23	26,5

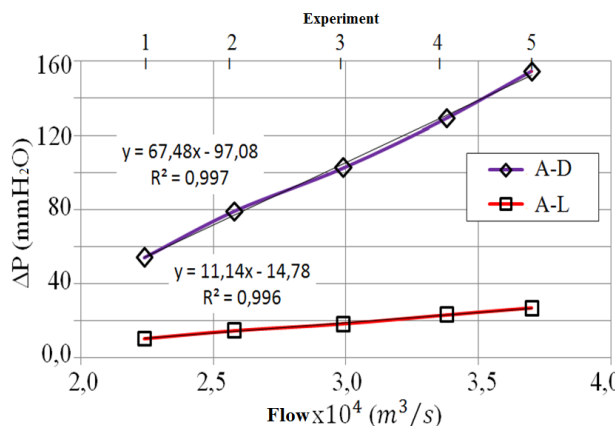


Figure 8. Trend lines and coefficient of determination R^2 .

During the operation of the pump, for taking the experimental readings there were vibrations in the test bench. Therefore, after an estimated time between four and six minutes, when the disturbances were minimum, it was proceeded to take the readings by direct observation of the level of each of the eleven water columns in the measurement unit of one millimeter, and a magnifying glass was used for amplifying the image when taking a reading of the water level located in the middle of the unit of one millimeter.

The obtained experimental results do not quantify the magnitude of the pressure between each reference, because they have a separation distance. Therefore, it is of interest to quantify and know the behavior in a continuous manner of the trajectory of the pressure profile along the walls of the Venturi tube, being of greatest interest between the references C and E, because this is the place where the largest pressure drops occur. For this purpose, the flow should be simulated through CFD, and thus know what could really happen.

3.2. Numerical results and comparison with the experimental data

The simulation of the velocity distribution of the isothermal flow in the Venturi tube is shown in Figure 9, both in the cross section and in the plane, where the increase of the velocity of the flow occurs in the throat, and the decrease in the divergent section. In the latter the contour lines of velocity acquire a parabolic profile in direction to the x axis, due to the effect of the boundary layer. The velocity of the flow is maximum in the axial symmetry of the x axis, and its magnitude decreases toward the walls of the Venturi tube, thus having a gradient of velocity in the flow field. It is worth noting that the domain of the flow shown in Figure 9, was simulated with structured mesh and quadrilateral cells, employing the standard $k - \epsilon$ turbulence model; since they are similar, other figures of the contour lines of velocity for the results of the standard $k - \omega$ turbulence model are not shown.

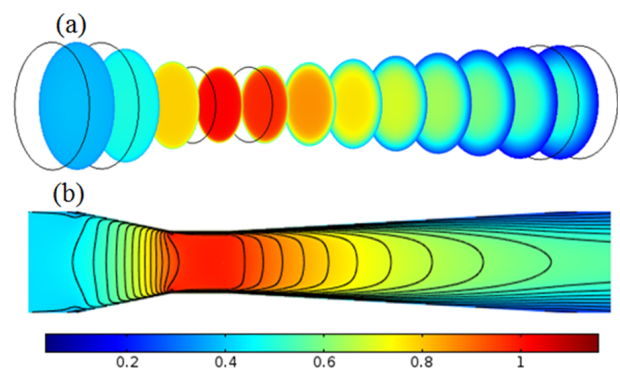


Figure 9. Distribution of velocity (m/s). (a) In the cross section, and (b) Projected on the plane.

Figure 10 shows the behavior of the velocity profiles evaluated in the axial symmetry of the x axis. According to all the trajectories of the profiles, toward the end of the convergent section the flow increases its velocity, in the throat section reaches a maximum velocity in the reference D, and decreases its velocity in the divergent section. The magnitude of the velocity of the flow in the reference A is smaller with respect to the reference L, thus it is understood that the behavior of the profile of the flow velocity in the radial direction has smaller curvature in the reference A, and larger curvature in the reference L.

The numerical results of the flow rates are shown in Table 7, for each turbulence model and type of mesh. The largest magnitude of flow rate was for the standard k-e turbulence model and domain meshed with quadrilateral cells, and the smallest flow rate for the standard k- ω turbulence model and domain meshed with triangular cells. It should be noted that the flow rate was determined with the average velocity of the flow, using the numerical integration method.

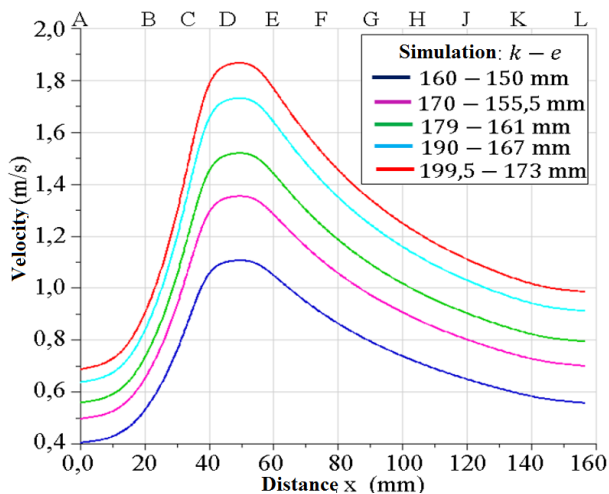


Figure 10. Profiles of velocity evaluated in the axial symmetry of the x axis, for the standard k-e turbulence model.

When the numerical flow rates presented in Table 7 are compared with the experimental values presented in Table 3, it can be seen that the greatest percentage error was 9.68 % for the standard k-e turbulence model and the domain meshed with quadrilateral cells, and 8.68 % for the mesh with triangular cells; the minimum percentage error was 1.48 % for the standard k-e and the mesh with quadrilateral cells, and 1.01 % for the standard k- ω and the mesh with triangular cells, as shown in Table 8. Based on the results, it is evident that there is an influence on the numerical results of the type of mesh applied to the computational domain.

Table 7. Flow rates obtained for two turbulence models and two types of applied meshes

Simulation (mm H ₂ O)	Flow rate $\times 10^4$ (m ³ /s)			
	Quadrilateral c.		Triangular c.	
	k-e	k- ω	k-e	k- ω
160-150	2,29	2,27	2,28	2,26
170-155,5	2,83	2,8	2,8	2,78
179-161	3,19	3,16	3,15	3,12
190-167	3,65	3,61	3,6	3,56
199,5-173	3,94	3,89	3,88	3,84

Table 8. Percentage error of the flow rates

Exp	Simulation (mm H ₂ O)	Percentage error (%)			
		Quadrilateral C.		Triangular C.	
		k-e	k- ω	k-e	k- ω
1	160-150	2,33	1,48	1,73	1,01
2	170-155,5	9,68	8,64	8,68	7,72
3	179-161	6,74	5,68	5,56	4,57
4	190-167	7,93	6,76	6,5	5,46
5	199,5-173	6,47	5,14	4,9	3,85

The numerical results of Reynolds number obtained for the greatest diameter in the references A and L are shown in Table 9, and for the smallest diameter in the reference D are shown in Table 10. In the references A and L, for the five simulations, the Reynolds number was in the range $12100 < Re < 21200$; and in the reference D, in the range $19700 < Re < 34400$. After comparing the numerical results of the Reynolds number presented in Tables 9 and 10, with respect to the experimental values of the Reynolds number presented in Table 4, the percentage error was in the range 1.02-9.68 %.

Table 9. Reynolds numbers obtained in the greatest diameter, in the references A and L, for two turbulence models and two types of applied meshes

Simulation (mm H ₂ O)	Reynolds Numbers in the references A y L			
	Quadrilateral C.		Triangular C.	
	k-e	k- ω	k-e	k- ω
160-150	12303	12201	12231	12144
170-155,5	15179	15034	15041	14908
179-161	17106	16935	16917	16758
190-167	19558	19345	19298	19109
199,5-173	21130	20866	20818	20610

Table 10. Reynolds numbers obtained in the smallest diameter, in the reference D, for two turbulence models and two types of applied meshes

Simulación (mm H ₂ O)	Reynolds Numbers in the reference D			
	Cuadrilateral C.		Triangular C.	
	<i>k-e</i>	<i>k-ω</i>	<i>k-e</i>	<i>k-ω</i>
160-150	19992	19827	19875	19735
170-155,5	24666	24431	24442	24226
179-161	27797	27519	27490	27231
190-167	31781	31436	31359	31053
199,5-173	34336	33907	33829	33492

Figure 11 shows the pressure distributions on the surface of the walls of the convergent, throat and divergent sections, and also the pressure distribution of the internal flow projected on the plane, with the contour lines which are the isobar, and it can be observed how the pressures are distributed in a manner perpendicular to the x axis and toward the walls.

The profiles of the gauge pressures obtained at the walls of the Venturi tube are shown in Figures 12 to 16. The unit of the pressure is millimeters of water column (mmH₂O), and the same graphs include the pressure data of the experiments that were carried out. The pressure profiles correspond to a domain meshed with quadrilateral cells, and for another domain meshed with triangular cells, with both cases simulated for isothermal flow with the turbulence models standard *k-e* and standard *k-ω*.

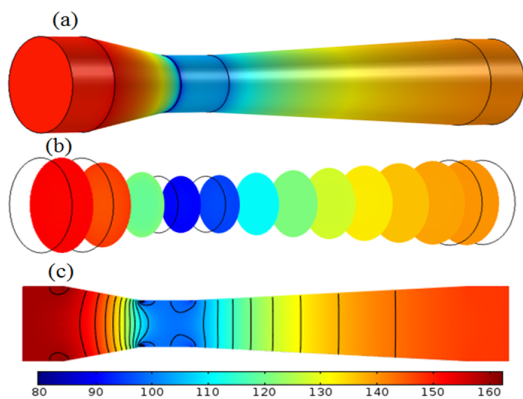


Figure 11. Pressure distribution (mm₂O). (a) On the surface of the wall, (b) On the cross section, and (c) Projected on the plane.

A simultaneous observation of Figures 12 to 16 shows that all pressure profiles have a similar behavior along the walls of the Venturi tube, the experimental data are intercepted and bordered. At the end of the straight section of the inlet of the Venturi tube, the profiles show a pressure increase to a magnitude greater than the inlet pressure. In the vertex between the convergent section and the throat, which is located

at a distance of 38 mm, an abrupt pressure drop occurs, even yielding a negative pressure for the profile *k-e* with quadrilateral cells for the simulation of experiment 4, and the same happens for the profiles *k-e* and *k-ω* with quadrilateral cells for the simulation of experiment 5. Similarly, it occurs in the region of the other vertex located at the right end of the throat at a distance of 54 mm, with a pressure drop of lower intensity but without the presence of negative pressure.

In the throat section, a stretch of the profiles exhibits a convex behavior, separated one from the other, ending up in the following order from the bottom up: the profile *k-e* and the profile *k-ω*, both simulated for the domain of mesh with quadrilateral cells, followed by the profile *k-e* and the profile *k-ω*, both simulated for the domain of mesh with triangular cells. It is observed how the five experimental data of pressure in the reference D were ranked. The stretches of the trajectories of the profiles *k-e* with quadrilateral cells have closer approximation to the experimental data. It should be pointed out that the pressure drop in the throat occurs because the flow passes through the narrow section at a higher velocity, due to the large difference of the flow pressure between the inlet and the outlet of the Venturi tube.

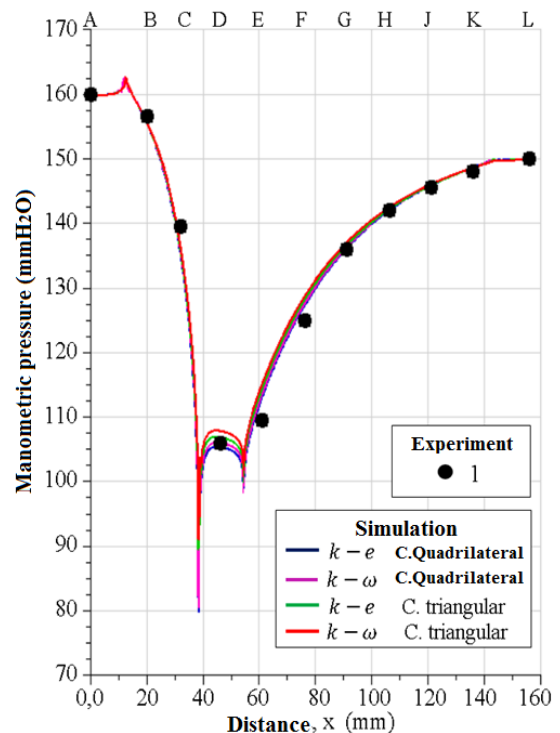


Figure 12. Experiment 1 of pressures of water columns, and pressure profiles evaluated at the wall of the Venturi tube. Pressure in (mmH₂O): 160 mm at the inlet and 150 mm at the outlet.

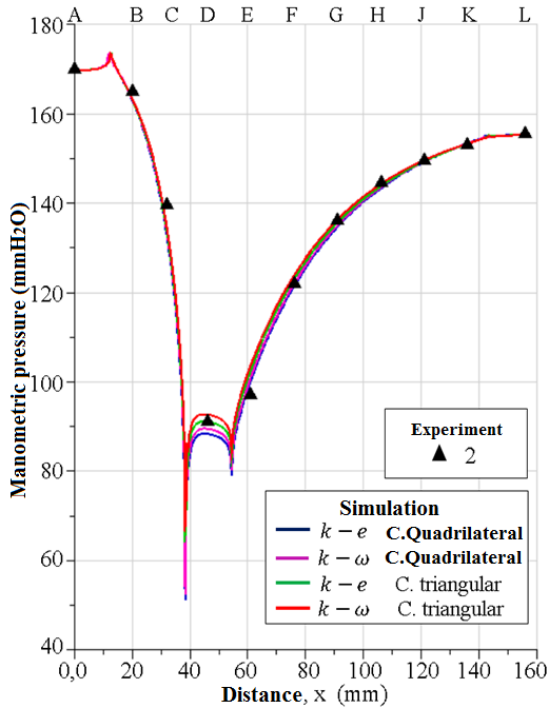


Figure 13. Experiment 2 of pressures of water columns, and pressure profiles evaluated at the wall of the Venturi tube. Pressure in (mmH₂O): 170 mm at the inlet and 155.5 mm at the outlet.

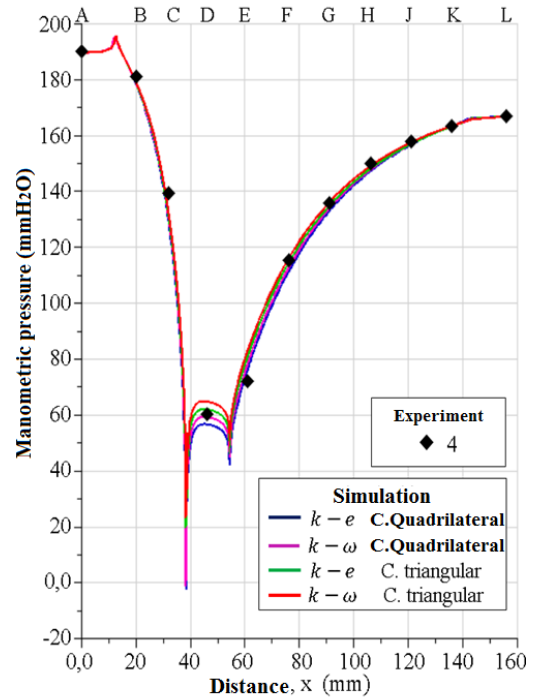


Figure 15. Experiment 4 of pressures of water columns, and pressure profiles evaluated at the wall of the Venturi tube. Pressure in (mmH₂O): 190 mm at the inlet and 167 mm at the outlet.

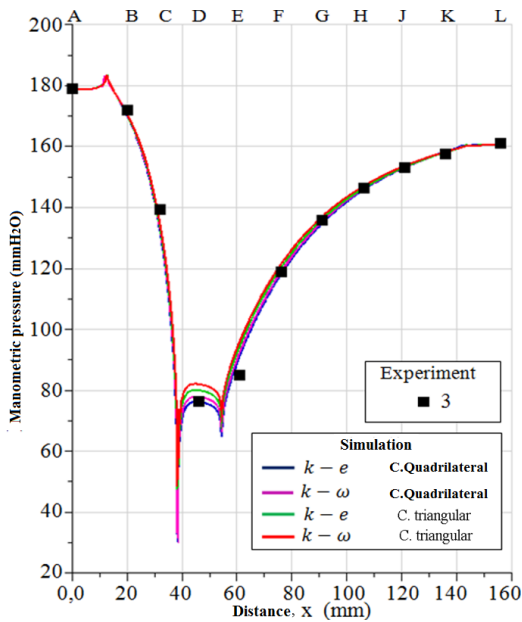


Figure 14. Experiment 3 of pressures of water columns, and pressure profiles evaluated at the wall of the Venturi tube. Pressure in (mmH₂O): 179 mm at the inlet and 161 mm at the outlet.

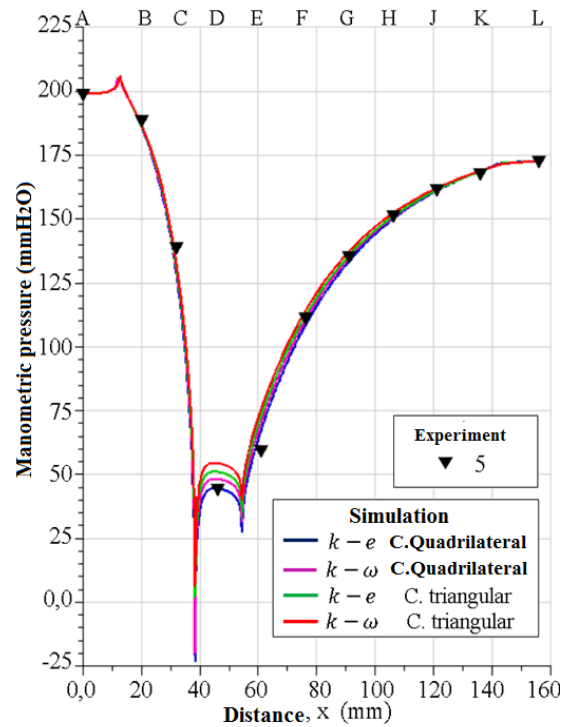


Figure 16. Experiment 5 of pressures of water columns, and pressure profiles evaluated at the wall of the Venturi tube. Pressure in (mmH₂O): 199.5 mm at the inlet and 173 mm at the outlet.

The numerical results and the experimental data in the reference D are shown in Table 11. The standard $k-e$ turbulence model showed the greatest percentage error of 5.88 % for experiment 4, for the standard $k-\omega$ it was 7.84 % for experiment 5, and values smaller than these for the remaining results, i.e. for the mesh with quadrilateral cells. On the other hand, for the mesh with triangular cells, corresponding to experiment 5, the standard $k-e$ had a percentage error of 14.17 %, for the standard $k-\omega$ it was 21.66 %, and smaller for the remaining results.

Table 11. Experimental and numerical data for the reference D, for two turbulence models and two types of applied meshes

Data Exp. Ref. D mmH ₂ O	Simulation: Reference D (mmH ₂ O)				
	Cell Quadrilateral		Cell Triangular		
	$k-e$	$k-\omega$	$k-e$	$k-\omega$	
1	106	105,47	106,13	106,99	107,97
2	91	88,51	89,66	91,28	92,86
3	76,5	76,4	78,05	80,22	82,26
4	60,5	56,94	59,57	62,32	65,11
5	45	44,79	48,53	51,38	54,75

The pressure profiles for the standard $k-e$ turbulence model, simulating the flow with the domain meshed with quadrilateral cells, and the experimental data of pressure presented in Table 5 and plotted in Figure 6, are presented in Figure 17, where it is observed that the trajectories of the profiles satisfy the validation with the experimental data. In the reference D located at the throat section, the trajectories of the profiles are convex. Although a graph similar to Figure 17 is not presented for the standard $k-\omega$ turbulence model, this model also shows validity but with slightly varied margins of numerical results with respect to the standard $k-e$ turbulence model, as shown in the results of Table 12 previously presented. From the analysis that was carried out, the numerical results are influenced by the type of mesh applied to the computational domain, and the structured mesh with quadrilateral cells provides more accurate numerical results compared to the mesh with triangular cells.

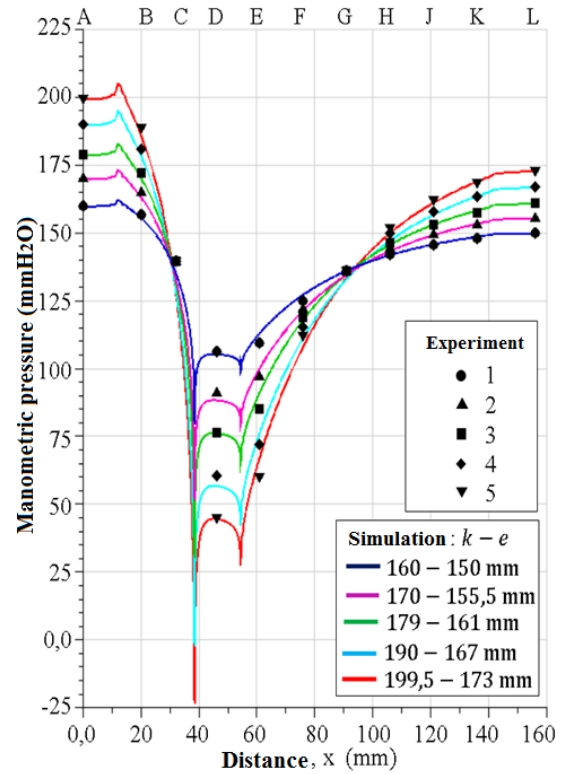


Figure 17. Experimental data of pressure of water columns and pressure profiles evaluated at the walls of the Venturi tube with the standard $k-e$ turbulence model

The pressures of the flow along the axial symmetry of the x axis, compared with the experimental data of the pressures on the walls of the Venturi tube, are shown in Figure 18. The profiles intercept with one another in the references C and G, and it is observed the evolution of the pressure drop trajectories in the left end of the reference D and of the pressure increase in the right end of the same reference; the trajectories of the curves are concave along the throat section. The small separations of the profiles of the experimental data are also shown, thus the magnitudes of the pressures in each of the references are some slightly greater and others slightly smaller with respect to the experimental data of the pressures on the walls. The profiles were obtained for the domain meshed with quadrilateral cells and the standard $k-e$ turbulence model.

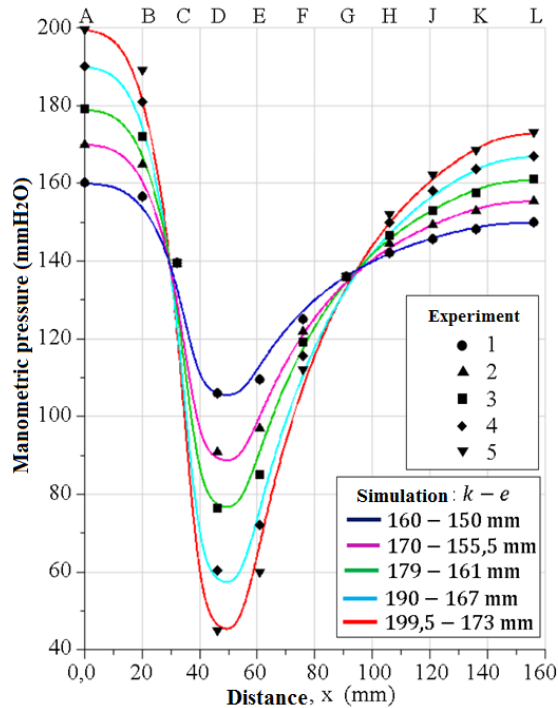


Figure 18. Experimental data of pressure of water columns and pressure profiles evaluated at the axial symmetry (x axis) of the Venturi tube with the standard $k - e$ turbulence model.

When the numerical results of Figure 18 are compared with Figure 17, it is evident that for the locations of the references A, B, C, D, E, F, G, H, J, K and L, the pressures tend to be perpendicular to the x axis and to the walls, forming a trajectory of curves known as isobars. However, in the places where the sections come together, in the vertices, the configuration of the trajectories of the curves has a different behavior due to the sharp variations of pressures, induced by the geometrical profile of the section of gradual contraction and gradual expansion of the Venturi tube.

Figure 19, as a detail, unifies Figures 17 and 18, for the distance range 30-100 mm, showing superimposed profiles stretches for the pressures on the walls and on the x axis, which are compared with the experimental data for the references C, D, E, F and G. It is observed the pressure drops at the ends of the throat and how the curves intercept and border the experimental data. It is shown that the abrupt drops of the numerical pressures on the wall occur for the 38.67 mm position, at the beginning of the throat; and the other pressure drops occurs at the 54.49 mm position, which is located at the beginning of the divergent section.

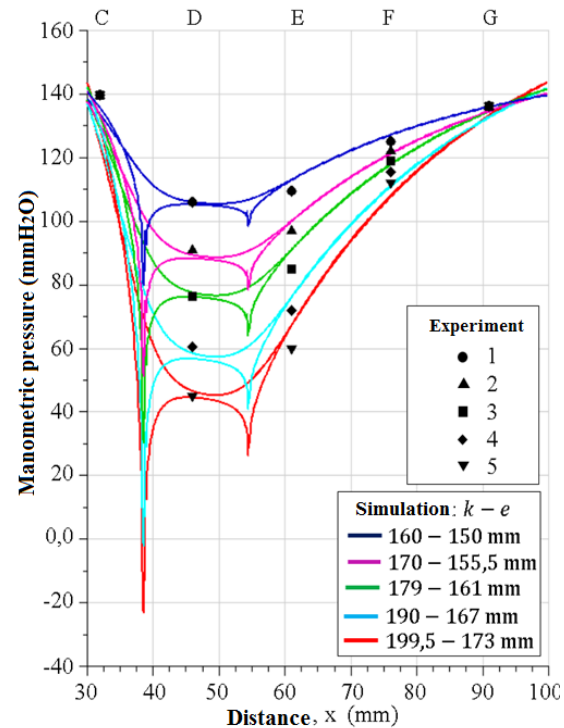


Figure 19. Experimental data for the references C, D, E, F and G, and stretches of pressure profiles evaluated at the walls and at the x axis of the Venturi tube with the standard $k - e$ turbulence model

Table 12 shows the numerical values of the pressure drops at the wall at the ends of the throat section. It is shown that the smallest drop of numerical pressure occurs at the 38.67 mm position, for the curve 199.5-173 mm which corresponds to experiment 5, being the magnitude of the pressure drop -23.23 (mmH₂O), and since it is a negative pressure, it is evident that it is a suction pressure; similarly, for the curve 190-167 mm corresponding to experiment 4 and for the same position, the pressure was -2.08 (mmH₂O).

The vertex, where the negative pressure occurs, corresponds to a very small part of an estimated radius of action of 0.2 mm, where the negative pressure is an unexpected result, because the hydrodynamic profile of the internal wall of the Venturi tube that measures the flow rate, the convergent section has an average angle of design with the purpose of avoiding negative pressures.

Table 12. Pressure drops at the ends of the throat

Numerical profile $k - e$	Position 38,67 mm mmH_2O	Position 54,49 mm mmH_2O
160-150 mm	79,75	98,94
170-155,5 mm	51,23	79,08
179-161 mm	30,17	64,73
190-167 mm	-2,08	42,07
199,5-173 mm	-23,23	27,63

Similarly, it is remarked that during experiments 4 and 5 no air bubbles were observed in the region around the vertex located at the inlet of the throat section and downstream, as a sign of cavitation. Therefore, the numerical result of the negative pressure, induces to investigate with sensitive instruments to capture the possible air bubbles with dimensions imperceptible to the human eye that might be present. Therefore, it should be verified simulating the flow with different turbulence models in a future work, to determine if negative pressures appear or not, thus obtaining conclusions close to the reality of the physical phenomenon.

From a comparison of the numerical results with the experimental data, it is evident that the simulation yields satisfactory results sustained by the ranges of error which are acceptable according to engineering criteria; thus the standard $k - e$ and standard $k - \omega$ turbulence models are validated. These two validated turbulence models strengthen their application in the computational fluid dynamics in the simulation of the flow in computational domains with simple or complex geometries in the field of engineering, and allow to determine the magnitude of some physical parameter that cannot be obtained through measuring instruments and analytical equations.

4. Conclutions

Based on the analyses that were carried out, for the cases of experimental and numerical study, it is concluded that:

The obtained numerical flow rates for the standard $k - e$ and standard $k - \omega$ turbulence models, when compared to the five experimental data of flow rates, yielded percentage errors in the range 1.01-9.68 %. Similarly, it was determined the percentage error in the range 1.01-9.68 % for the Reynolds number. For the five experiments, the Reynolds number is in the range $12000 < Re < 32300$; and for the numerical simulations, in the range $12100 < Re < 34400$.

The five experimental results of the pressures obtained in the references C and G, where the diameters of the Venturi tube are different, show that the magnitude of the pressures in that place do not vary, even

though the velocity of the flow increases in such references due to the increase in the flow rate. Besides, the smallest pressure drop occurs in the middle part of the throat section because of the Venturi effect.

Regarding the profiles obtained with the standard $k - e$ and standard $k - \omega$ turbulence models, which were compared with the experimental data of pressure, the standard $k - e$ turbulence model with the domain meshed with quadrilateral cells gave the more accurate result, where the numerical results fitted better the experimental data in the middle part of the throat section, which is a critical section due to the abrupt drop in the fluid pressure. This evidences that the type of mesh influences the numerical results.

At the ends of the throat section, at the 38.67 mm and 54.49 mm positions, the pressure drops were more abrupt than in the middle part of the throat, appearing negative pressures at the 38.67 mm position for the numerical curves corresponding to experiments 4 and 5.

The smallest pressure drop at the wall does not occur in the middle part of the throat section, but at the ends of it, for the Venturi tube under study.

In future works, for experimental studies of the same type of Venturi tube, it is recommended to manipulate the control valve, and with the obtained experimental results, carry out the corresponding comparisons with the experimental results of the present work. Similarly, for cases of numerical studies, it is recommended to utilize other codes of CFD to simulate the flow of water employing other turbulence models, and compare with the numerical results of the present work.

Acknowledgements

My gratitude to Jehovah, my almighty God, my source of wisdom and inspiration. To the Mechanical Engineering Department of the National Experimental Polytechnic University “AJS”, Puerto Ordaz Vice-Rectorate, Bolívar, Venezuela. To the Group of Mathematical Modeling and Numerical Simulation (GMMNS) of the National University of Engineering (NUE), Lima, Peru.

References

- [1] F. M. White, *Mecánica de fluidos*, M.-H. I. de España S.L., Ed., 2004. [Online]. Available: <https://bit.ly/2MYFv6r>
- [2] Y. A. Çengel and J. M. Cimbala, *Mecánica de fluidos, fundamentos y aplicaciones*, M.-H. I. de España S.L., Ed., 2006. [Online]. Available: <https://bit.ly/2BUeJWD>
- [3] H. S. Bean, “Fluid meters their theory and application- sixth edition,” The American Society

- of Mechanical Engineers (ASME), Tech. Rep., 1971. [Online]. Available: <https://bit.ly/33c2OiM>
- [4] “Invention of the venturi mete,” *Nature*, no. 136, p. 254, 1935. [Online]. Available: <https://doi.org/10.1038/136254a0>
- [5] O. Reynolds, “An experimental investigation of the circumstances which determine whether the motion of water shall be direct or sinuous, and of the law of resistance in parallel channels author(s): Osborne reynolds,” *Philosophical Transactions of the Royal Society of London*, vol. 174, pp. 935–982, 1883. [Online]. Available: <https://bit.ly/3211iyT>
- [6] N. Rott, “Note on the history of the reynolds number,” *Annual Review of Fluid Mechanics*, vol. 22, no. 1, pp. 1–12, 1990. [Online]. Available: <https://doi.org/10.1146/annurev.fl.22.010190.000245>
- [7] J. H. Ferziger and M. Peric, *Computational Methods for Fluid Dynamics*, 3rd ed., S.-V. B. H. N. York, Ed., 2002. [Online]. Available: <https://doi.org/10.1007/978-3-642-56026-2>
- [8] D. C. Wilcox, *Turbulence modeling for CFD*, I. DCW Industries, Ed., 1993. [Online]. Available: <https://bit.ly/2Pxxkdf>
- [9] T. V. Karman, “The fundamentals of the statistical theory of turbulence,” *Journal of the Aeronautical Sciences*, vol. 4, no. 4, pp. 131–138, 1937. [Online]. Available: <https://doi.org/10.2514/8.350>
- [10] H. Schlichting and K. Gersten, *Boundary-layer theory*, S.-V. B. Heidelberg, Ed., 2017. [Online]. Available: <https://doi.org/10.1007/978-3-662-52919-5>
- [11] D. Lindley, “An experimental investigation of the flow in a classical venturimeter,” *Proceedings of the Institution of Mechanical Engineers*, vol. 184, no. 1, pp. 133–160, 1969. [Online]. Available: https://doi.org/10.1243/PIME_PROC_1969_184_015_02
- [12] J. A. Sattery and M. J. Reader-Harris, “Computation of flow through venturi meters,” *North Sea Flow Measurement Workshop*, 1997. [Online]. Available: <https://bit.ly/2q2oZcT>
- [13] N. Tamhankar, A. Pandhare, A. Joglekar, and V. Bansode, “Experimental and cfd analysis of flow through venturimeter to determine the coefficient of discharge,” *International Journal of Latest Trends in Engineering and Technology (IJLTET)*, vol. 3, no. 4, pp. 194–200, 2014. [Online]. Available: <https://bit.ly/2Nmabh6>
- [14] B. E. Launder and D. B. Spalding, *Lectures in mathematical models of turbulence*, A. P. London, New York, Ed., 1972. [Online]. Available: <https://bit.ly/2qWgZud>
- [15] D. C. Wilcox, “Reassessment of the scale-determining equation for advanced turbulence models,” *AIAA Journal*, vol. 26, no. 11, pp. 1299–1310, 1988. [Online]. Available: <https://doi.org/10.2514/3.10041>
- [16] G. Alfonsi, “Reynolds-averaged navier-stokes equations for turbulence modeling,” *Applied Mechanics Reviews*, vol. 62, no. 4, p. 040802, 2009. [Online]. Available: <https://doi.org/10.1115/1.3124648>